IEEE Open Journal of Vehicular Technology

Received 2 March 2023; accepted 3 April 2023. Date of publication 5 April 2023;
date of current version 24 April 2023. The review of this article was coordinated by Editor Tianqi Mao.

Digital Object Identifier 10.1109/OJVT.2023.3264879

An Asymptotic Framework for Fox's H-Fading Channel With Application to Diversity-Combining Receivers

PUSPRAJ SINGH CHAUHAN [1], SANDEEP KUMAR [2] (Senior Member, IEEE), ANKIT JAIN [1], AND LAJOS HANZO [3] (Life Fellow, IEEE)

[1]Department of Electronics & Communication Engineering, Pranveer Singh Institute of Technology, Kanpur 209305, India
[2]Central Research Laboratory, Bharat Electronics Limited, Gaziabad 201010, India
[3]School of Electronics and Computer Science, University of Southampton, SO17 1BJ Southampton, U.K.

CORRESPONDING AUTHOR: LAJOS HANZO (e-mail: lh@ecs.soton.ac.uk).

The work of Lasoj Hanzo was supported in part by Engineering and Physical Sciences Research Council Projects under Grants EP/W016605/1 and EP/X01228X/1 and in part by European Research Council's Advanced Fellow Grant QuantCom under Grant 789028.

ABSTRACT Unified statistics are valuable in the performance analysis of communication systems. In this context, Fox's H-function has been shown to be eminently suitable for diverse scenarios. Another pivotal requirement is to have a low computational complexity, which is often hard to achieve for generalized models. Given this motivation, in this article we have presented high-power, low-complexity solutions for the outage probability (OP) and the average symbol error probability (SEP). Additionally, diversity techniques are harnessed for mitigating the effect of fading, which are then analysed based on the results derived. The entire methodology is governed by the origin probability density function rather than approximating the performance metrics under high-power. All the presented mathematical expressions are compared and validated through computer simulations (Monte-Carlo) to verify the accuracy of the proposed framework.

INDEX TERMS Asymptotic analysis, diversity reception, error probability, Fox's H-fading, outage probability.

I. INTRODUCTION

Given the availability of generalised distributions like α-μ, η-μ, κ-μ, α-η-μ, α-η-μ, α-κ-μ, etc., the need for having unified statistics is increasing day by day. In this context, Fox's H-function has grown in popularity because of its versatile nature and elegant form in terms of representing most of the earlier proposed fading channels [1]. The distribution offers significant flexibility in characterizing numerous fading models [2, Table I].The measurement and modeling campaigns have evidenced that the multipath fading of the V2V channel at 5 GHz and 5.2 GHz can be closely modelled by the generalized Fox's H-function distribution. The model encompasses the various other typical models of vehicular and D2D propagation scenarios such as Rayleigh, Nakagami-m, Fisher-F (at 5.8 GHz for D2D application), Weibull etc. [3], [4], [5].

Various researchers have proposed novel frame-works for analysing the performance of wireless systems relying on Fox's H-fading [1], [2], [6], [7], [8], [9], [10]. In this regard, Yilmaz et al. [6] has presented a methodology for deriving the closed-form expressions of the average BEP and average capacity for transmission over the Hyper Fox's H-fading model expressed in terms of Fox's H-function. The evaluation of the average BEP and average capacity expressions routinely utilize the MGF based approach for both single and multiple links. In [7], [8], the channel capacity is derived both with and without delay constraints for different adaptive schemes relying on optimal rate adaptation, on optimal power, on channel inversion, and on truncated channel inversion at a fixed rate over Fox's H-fading channel. Abo Rahama et al. [1] derived novel results for the PDF and CDF over the sum of Fox's H-function utilizing the MGF-based approach. They also utilized these results for evaluating the OP, average BEP, and ergodic capacity of wireless system. Physical layer statistics have been presented for transmission over Fox's H wiretap fading channel in [9], where the eavesdropper may be colluding or non-colluding. In case of a colluding scenario, the

TABLE 1. Contrasting our contributions to the literature of Fox H-fading channels.

Parameters	[1]	[2]	[9]	[10]	[22]	[23]	[24]	[25]	[26]	This work
i.i.d. Branches					✓			✓	✓	✓
i.n.i.d. Branches	✓									✓
MRC diversity	✓							✓	✓	✓
Outage probability	✓				✓		✓			✓
Average SEP	✓						✓		✓	✓
Effective capacity						✓				
Ergodic capacity	✓						✓		✓	
Physical Layer Security parameters			✓		✓					
Spectrum sensing parameters		✓		✓				✓		
Diversity gain				✓						✓
AWGN	✓	✓	✓	✓	✓	✓	✓	✓	✓	✓
Laplacian noise										✓
Origin PDF-based approach				✓				✓	✓	✓
Function approximation under High SNR-based approach	✓	✓	✓		✓	✓	✓			
EGC diversity										✓
SC diversity										✓

eavesdropper is equipped with MRC and SC schemes. The validity of the proposed formulation has been verified under different fading environments. The results presented in [9] subsumed the results presented in previous treatises. Furthermore, El Ayadi [2] and Chauhan et al. [10] derived cognitive radio performance metrics for transmission over Fox's H-fading under different propagation environments. In [1], [2], [6], [7], [8], [9], [10] the performance metrics relied either on univariate, bivariate, or multivariate Fox's H-functions. However, the earlier analytics may limit the operating range due to instabilities, while evaluating these expressions by numerical integration. Furthermore, they may fail to provide a visual interpretation of how the system reacts to time-variant changes in channel and system characteristics. Therefore, it is usually desired to find simpler expressions for the quantities of interest.

To address these concerns, the research community turned to asymptotic analysis at high SNR [11], [12], [13], [14]. This approach results in computational simplicity and allows us to analyse the variations of statistics by relying on the average SNR. It also helps in comparing the performance of various modulation schemes. This approach has been frequently invoked [1], [2], [10], [11], [12], [13], [14]. Specifically, the asymptotic results derived for various metrics are discussed both for SISO and SIMO scenarios [1], [2], [10]. The high-power expressions of the average bit error or symbol error probabilities are evaluated in [1]. Similarly, the average probability of detection and average area under the receiver's operating characteristic curve are also derived in [1].

The recent works on the asymptotic analysis over Fox H-fading channels have been listed in Table 1. Although, the asymptotic analysis of different system performance metrics was presented for Fox H-fading channels, most of the analysis was carried out for single-branch Rxs. Only [1] has considered the asymptotic analysis of Fox H-fading channels for MRC diversity, but the results derived are not in generic form. Explicitly, the average SEP expressions were found using (13) of [15], which is only applicable for BPSK and BFSK. The asymptotic outage and ergodic capacity expressions do not rely on simple functions, but due to the presence of multiple summation terms required for MRC diversity, substantial computation is required for their evaluation. Furthermore, it is noted from Table 1, that none of the previous contributions have analysed EGC and SC diversity for Fox H-fading channels. Although EGC is suboptimal, it benefits from simpler channel estimation, which only requires estimation of the channel phase, but not the channel amplitude [16]. Due to the complex circuitry of the MRC, the EGC is often preferred in 5 G applications, including V2V and D2D communication. Hence the asymptotic analysis of Fox H-fading channel is the need of the hour. Furthermore, none of the previous works have considered Laplacian noise in their analysis, which is essentially used for satisfying the differential privacy that prevents information leakage in secure applications, indoor, outdoor, free-space optics and undersea communication environments [17], [18], [19], [20], [21].

In an attempt to fill these knowledge gaps, we have carried out the asymptotic analysis of Fox-H fading channels for various diversity combining techniques. The application of the resultant formulas in deriving the generic expressions of the performance metrics has been demonstrated. We have considered both the ubiquitous AWGN and ALN. By contrast, the system considered here has multiple Rx antennas along with diverse combining schemes such as MRC, EGC, and SC. In this treatise, we have focused on a PDF-based approach. The main contributions of this work are summarised as follows:

- New expressions are derived for different diversity combining techniques, relying on both i.i.d and independent as well as on non-identically distributed branches.
- Explicitly, analytical expressions are derived for both the OP and for the average SEP. Furthermore, unified error probability statistics are obtained for both coherent and non-coherent schemes in AWGN scenarios. Additionally, the error probability of coherent modulation schemes is evaluated in the face of ALN.
- The final BER and OP expressions are articulated with the aid of computationally convenient asymptotes.

TABLE 2. Nomenclature.

5G	Fifth Generation
A2G	Air-to-Ground
ALN	Additive Laplacian Noise
AWGN	Additive White Gaussian Noise
α-μ/G	α-μ/Gamma
BEP	Bit Error Probability
BFSK	Binary Frequency Shift Keying
BPSK	Binary Phase-Shift Keying
CDF	Cumulative Distribution Function
D2D	Device-to-Device
DSS	Double Shadowed Scenario
EGC	Equal Gain Combining
EGK	Extended Generalized-K
EG-G	Extended Generalized Gamma
F-S	Fisher-Snedecor
G2A	Ground-to-Air
GBK	Generalised Bessel-K
GK	Generalised-K
i.i.d.	Independent and Identically Distributed
i.n.i.d.	Independent and Non-Identically Distributed
LT	Laplace Transform
MED	Minimum Euclidian Distance
MGF	Moment-Generating Function
MIMO	Multiple-Input Multiple-Output
MRC	Maximum-Ratio Combining
OP	Outage Probability
PAM	Pulse Amplitude Modulation
PDF	Probability Density Function
PSK	Phase-Shift Keying
QoS	Quality-of-Service
QPSK	Quadrature Phase Shift Keying
RMS	Root-Mean-Square
Rx	Receiver
SAGIN	Space-Air-Ground Integrated Network
SC	Selection Combining
SEP	Symbol Error Probability
SIMO	Single-Input Multiple-Output
SISO	Single-Input Single-Output
SNR	Signal-to-Noise Ratio
SSS	Single Shadowed Scenario
Tx	Transmitter
V2V	Vehicle-to-Vehicle

TABLE 3. Notations.

α	Non-linearity parameter
μ	Number of multipath cluster
γ	Instantaneous received SNR
$\bar{\gamma}$	Average received SNR
$\hat{r}$	Fading figure of EG-G distribution
ξ	Shaping factor of EG-G distribution
$\hat{r}_s$	Shadowing severity of EG-G distribution
ξ_s	Shadowing inhomogeneity of EG-G distribution
$\Gamma(.)$	Gamma function
$\hat{n}$	Fading severity of F-S F distribution
$\hat{m}$	Shadowing severity of F-S F distribution
n_G, m_G, & $\hat{\lambda}$	Shaping factors of GBK distribution
δ	Path loss exponent
D	Tx and Rx separation
$\hat{k}$	Shape parameter for Gamma distribution
$\hat{\Omega}$	Average power of α-μ distribution
m_i, $\{i = 1, 2\}$	Nakagami-m fading parameters
a_i, $\{i = 1, 2\}$	Shaping parameter of Inverse Gamma distribution
$\tilde{m}_i$ & $\tilde{m}_{si}$, $\{i = 1, 2\}$	Shape parameters of GK distribution
P_t	Transmitted power
E	Instantaneous propagation loss
N_0	Noise power
Ω_{si},$\{i = 1, 2\}$	Mean power of GK distribution
$\tilde{\xi}$	Ratio of equivalent beam radius and pointing error displacement standard deviation at the Rx
r	Detection parameter for Gamma-Gamma distribution
ς & ϖ	Scintillation parameters of the atmospheric turbulence
μ_{R_D}	average SNR for Gamma-Gamma distribution
L	Number of independent parallel paths
γ_r	r^{th} branch instantaneous received SNR
$M_{\gamma_r}(s)$	MGF of r^{th} branch instantaneous received SNR
γ_{MRC}	Instantaneous received SNR at the output of MRC detector
γ_{EGC}	Instantaneous received SNR at the output of EGC detector
γ_{SC}	Instantaneous received SNR at the output of SC detector
$M_{X_r}(s)$	MGF of r^{th} branch envelope
$f_Y(\gamma)$	PDF of received SNR
$F_{\gamma_r}(\gamma)$	r^{th} branch CDF
γ_{th}	Threshold SNR
$P_{out}(.)$	Probability of outage
$erfc(.)$	Complementary error function
$P_e(.)$	Instantaneous SEP
$\bar{P}_e$	Average SEP

Simulations are conducted to validate the accuracy of the results produced, which are accurate at high-SNRs.

The results derived here are beneficial as they (i) yield a unified mechanism for the average SEP and OP associated with multiple branches; (ii) serve as an efficient potential tool for analysing the system performance, when the channel characteristics are acquired by Fox's H module or in the analysis of special cases, which have hitherto not been taken into consideration. For easy referencing, all the acronyms and variables used throughout the work are defined in Table 2 and Table 3, respectively. The rest of the paper is organised as follows: In Section II, the general Fox channel model is covered in detail, and a few unique Fox H-fading channel examples are taken into consideration. The methodology of handling different diversity schemes is elaborated on in Section III. In Section IV, asymptotic results are provided for the OP and the average SEP under both AWGN and ALN scenarios. Section V verifies the accuracy of the results. Finally, Section VI summarizes the paper.

II. FOX'S H-FADING CHANNEL

In the literature, Fox's H representation is often used to characterize the channels in wireless propagation environments [1], [2], [10], because it subsumes well-known distributions modelling the practical propagation channels [6]. These channels include the Rayleigh, Maxwell, Weibull, Gamma, Weibull, Nakagami-m, GK, EGK, EG-G, F-S-F, Nakagami-m/Gamma, scenarios as their special cases [2], [6], [9]. The model's practical utility can be found in a variety of applications, including vehicle-to-vehicle and keyhole MIMO

TABLE 4. Unique distribution examples of Fox's H-function.

Channel	$f_Y(\gamma)$
Maxwell [2, Table I]	$f_Y(\gamma) = \frac{3}{\sqrt{\pi}\bar{\gamma}} H_{0,1}^{1,0}\left[\frac{3\gamma}{2\bar{\gamma}}\middle\vert \begin{matrix} - \\ (\frac{1}{2};1) \end{matrix}\right]$
α-μ [9, Table I]	$f_Y(\gamma) = \frac{\mu^{\frac{2}{\alpha}}}{\Gamma(\mu)\bar{\gamma}} H_{0,1}^{1,0}\left[\frac{\mu^{\frac{2}{\alpha}}\gamma}{\bar{\gamma}}\middle\vert \begin{matrix} - \\ (\mu-\frac{2}{\alpha};\frac{2}{\alpha}) \end{matrix}\right]$, $\alpha>0$ & $\mu>0$
EG-G [6, Table II]	$f_Y(\gamma) = \frac{\beta\beta_s}{\Gamma(\hat{r})\Gamma(\hat{r}_s)\bar{\gamma}} H_{0,2}^{2,0}\left[\frac{\beta\beta_s}{\bar{\gamma}}\gamma\middle\vert \begin{matrix} - \\ (\hat{r}-\frac{1}{\xi},\frac{1}{\xi}),(\hat{r}_s-\frac{1}{\xi_s},\frac{1}{\xi_s}) \end{matrix}\right]$, $\beta=\Gamma(\hat{r}+1/\xi)/\Gamma(\hat{r})$ & $\beta_s=\Gamma(\hat{r}_s+1/\xi_s)/\Gamma(\hat{r}_s)$
F-S $\mathcal{F}$ [9, Table I]	$f_Y(\gamma) = \frac{\hat{n}}{\hat{m}\Gamma(\hat{n})\Gamma(\hat{m})\bar{\gamma}} H_{1,1}^{1,1}\left[\frac{\hat{n}\gamma}{\hat{m}\bar{\gamma}}\middle\vert \begin{matrix} (-\hat{m},1) \\ (\hat{n}-1,1) \end{matrix}\right]$
GBK [33]	$f_Y(\gamma) = \frac{1}{\Gamma(m_G)\Gamma(n_G)\Xi} H_{0,2}^{2,0}\left[\frac{\gamma}{\Xi}\middle\vert \begin{matrix} - & - \\ (m_G-\frac{1}{\lambda};\frac{1}{\lambda}) & (n_G-\frac{1}{\lambda};\frac{1}{\lambda}) \end{matrix}\right]$, $\Xi=\frac{\bar{\gamma}\Gamma(m_G)\Gamma(n_G)}{\Gamma(m_G+1/\hat{\lambda})\Gamma(n_G+1/\hat{\lambda})}$
α-μ/G [34]	$f_Y(\gamma) = \frac{\mu^{\frac{1}{\alpha}} D^{\delta}}{\Gamma(\mu)\Gamma(\hat{k})v\hat{\Omega}} H_{0,2}^{2,0}\left[\frac{\mu^{\frac{1}{\alpha}} D^{\delta}\gamma}{v\hat{\Omega}}\middle\vert \begin{matrix} - \\ (\mu-\frac{1}{\alpha},1)(\hat{k}-1,1) \end{matrix}\right]$, $2<\delta<6$
SSS [36]	$f_Y(\gamma) = \frac{\mathcal{A}_1 m_1 m_2}{\bar{\gamma}} H_{1,2}^{2,1}\left[\frac{m_1 m_2\gamma}{\bar{\gamma}}\middle\vert \begin{matrix} (-a_1,1) \\ (m_1-1,1)(m_2-1,1) \end{matrix}\right]$, $\mathcal{A}_1=\frac{1}{\Gamma(m_1)\Gamma(m_2)\Gamma(a_1)}$
DSS [36]	$f_Y(\gamma) = \frac{\mathcal{A}_2 m_1 m_2}{\bar{\gamma}} H_{2,2}^{2,2}\left[\frac{m_1 m_2\gamma}{\bar{\gamma}}\middle\vert \begin{matrix} (-a_2,1)(-a_1,1) \\ (m_1-1,1)(m_2-1,1) \end{matrix}\right]$, $\mathcal{A}_2=\frac{1}{\Gamma(m_1)\Gamma(m_2)\Gamma(a_1)\Gamma(a_2)}$
Cascaded G-K [35]	$f_Y(\gamma) = \mathcal{A}_3\mathcal{A}_4 H_{0,4}^{4,0}\left[\mathcal{A}_4\gamma\middle\vert \begin{matrix} - \\ (\tilde{m}_{s1}-1,1)(\tilde{m}_1-1)(\tilde{m}_{s2}-1,1)(\tilde{m}_2-1) \end{matrix}\right]$, $\mathcal{A}_3 = \frac{1}{\Gamma(\tilde{m}_1)\Gamma(\tilde{m}_2)\Gamma(\tilde{m}_{s1})\Gamma(\tilde{m}_{s2})}$ $\mathcal{A}_4 = \frac{\tilde{m}_1\tilde{m}_2\tilde{m}_{s1}\tilde{m}_{s2}}{\bar{\gamma}}$ & $\bar{\gamma} = \frac{P_t E}{N_0}\Omega_{s1}\Omega_{s2}$
Gamma-Gamma [37]	$f_Y(\gamma) = \frac{(\varsigma\varpi)^r \tilde{\xi}^2}{\mu_{R_D}\Gamma(\varsigma)\Gamma(\varpi)} H_{1,3}^{3,0}\left[\frac{(\varsigma\varpi)^r}{\mu_{R_D}}\gamma\middle\vert \begin{matrix} (\tilde{\xi}^2+1-r,r) \\ (\tilde{\xi}^2-r,r)(\varsigma-r,r)(\varpi-r,r) \end{matrix}\right]$
N*Rayleigh [38]	$f_Y(\gamma) = \frac{1}{\bar{\gamma}} H_{0,N}^{N,0}\left[\frac{\gamma}{\bar{\gamma}}\middle\vert \begin{matrix} - \\ (0,1)(0,1)----(0,1) \end{matrix}\right]$
N*Nakagami-m [39]	$f_Y(\gamma) = \frac{1}{\bar{\gamma}} H_{0,N}^{N,0}\left[\frac{\gamma}{\bar{\gamma}}\prod_{i=1}^{N}\Gamma(m_i)\middle\vert \begin{matrix} - \\ (m_1-1,1)(m_2-1,1)--(m_N-1,1) \end{matrix}\right]$
N*GK [40]	$f_Y(\gamma) = \frac{\prod_{i=1}^{N}\tilde{m}_i\tilde{m}_{si}}{\bar{\gamma}\prod_{i=1}^{N}\Gamma(\tilde{m}_i)\Gamma(\tilde{m}_{si})} H_{0,2N}^{2N,0}\left[\prod_{i=1}^{N}\frac{\Gamma(\tilde{m}_i)\Gamma(\tilde{m}_{si})\gamma}{\bar{\gamma}}\middle\vert \begin{matrix} - \\ (\tilde{m}_1-1,1)(\tilde{m}_{s1}-1,1)----(\tilde{m}_N-1,1)(\tilde{m}_{sN-1},1) \end{matrix}\right]$
N*Fisher [41]	$f_Y(\gamma) = \frac{1}{\bar{\gamma}\prod_{i=1}^{N}\Gamma(\hat{n}_i)\Gamma(\hat{m}_i-1)} H_{N,N}^{N,N}\left[\frac{\gamma}{\bar{\gamma}}\prod_{i=1}^{N}\frac{\Gamma(\hat{n}_i)}{\Gamma(\hat{m}_i-1)}\middle\vert \begin{matrix} (-\hat{m}_1,1)(-\hat{m}_2,1)---(-\hat{m}_N,1) \\ (\hat{n}_1-1,1)(\hat{n}_2-1,1)----(\hat{n}_N-1,1) \end{matrix}\right]$
N*α-$\mathcal{F}$ [31]	$f_Y(\gamma) = \frac{1}{\prod_{i=1}^{N}\Theta_i^{\frac{2}{\alpha_i}}\bar{\gamma}_i\Gamma(\mu_i)\Gamma(\hat{m}_i)} H_{N,N}^{N,N}\left[\frac{\gamma}{\prod_{i=1}^{N}\Theta_i^{\frac{2}{\alpha_i}}\bar{\gamma}_i}\middle\vert \begin{matrix} \Phi_1,\Phi_2,-----\Phi_N \\ \Upsilon_1,\Upsilon_2,-----\Upsilon_N \end{matrix}\right]$, $\Phi_i = (1-\hat{m}_i-2/\alpha_i, 2/\alpha_i)$ $\Theta_i = \frac{\hat{m}_i-1}{\mu_i}$ and $\Upsilon_i = (\mu_i-2/\alpha_i, 2/\alpha_i)$

systems [3], [27], G2A, and A2G unmanned aerial vehicle communications [28], millimeter-wave (i.e. ≥ 60 GHz) & free space optical communication [29], as well as D2D scenarios of indoor and outdoor environments [5]. Let the statistical variation of these real-world wireless communication environments follow Fox's H representation. Then the instantaneous power PDF is expressed as [2, equation (10)]

$$f_Y(\gamma) = \mathcal{R} H_{\hat{p},\hat{q}}^{\hat{m},\hat{n}}\left[\mathcal{T}\gamma\middle\vert \begin{matrix} (e_j,E_j)_{j=1..\hat{p}} \\ (f_j,F_j)_{j=1..\hat{q}} \end{matrix}\right],\ \gamma>0, \tag{1}$$

where the parameters $\hat{m}, \hat{n}, \hat{p}, \hat{q}$ posses positive integer values, and follow $0\leq\hat{m}\leq\hat{q}$, $0\leq\hat{n}\leq\hat{p}$. The constants $\mathcal{R}$ and $\mathcal{T}$ in (1) are adjusted to satisfy that $\int_0^{\infty} f_Y(\gamma)d\gamma = 1$. Equation (1) can alternatively be written in integral form as [30, equations. (1.2) & (1.3)]

$$\begin{aligned} f_Y(\gamma) &= \frac{\mathcal{R}}{2\pi i}\int_{\mathcal{L}} \Theta_{\hat{p},\hat{q}}^{\hat{m},\hat{n}}\left[s\middle\vert \begin{matrix} (e_j,E_j)_{j=1..\hat{p}} \\ (f_j,F_j)_{j=1..\hat{f}} \end{matrix}\right](\mathcal{T}\gamma)^{-s}ds, \\ &= \frac{\mathcal{R}}{2\pi i}\int_{\mathcal{L}}(\mathcal{T}\gamma)^{-s} \\ &\quad\times\frac{\prod_{j=1}^{\hat{m}}\Gamma(f_j+F_jS)\prod_{j=1}^{\hat{n}}\Gamma(1-e_j-E_js)}{\prod_{j=\hat{n}+1}^{\hat{p}}\Gamma(e_j+E_js)\prod_{j=\hat{m}+1}^{\hat{q}}\Gamma(1-f_j-F_jS)}ds, \end{aligned} \tag{2}$$

where $E_j>0$ for $j=1,...\hat{p}$ and $F_j>0$ for $j=1,...\hat{q}$ and the path of integration will be governed by the function's parameters. The $f_Y(\gamma)$ expressions are illustrated in Table 4 for the Maxwell, α-μ, EG-G [6], F-S-$\mathcal{F}$ [9], GBK, α-μ/G, SSS, DSS, cascaded G-K, Gamma-Gamma, N*Rayleigh, N*Nakagami-m, N*GK, N*Fisher, and N*α-$\mathcal{F}$ models for

ground-to-ground and A2G channels. The values of $\mathcal{R}$ and $\mathcal{T} > 0$ from the table may be determined for different fading models. Explicitly, in Table 4, we can see some special cases of Fox's H-fading models, which have already been introduced in the literature, such as the Maxwell, α-μ [9, Table I], E G-G [6, Table II], F-S $\mathcal{F}$ [9, Table I], and N*α-$\mathcal{F}$ [31] distributions. But others, such as, GBK is deduced by utilizing [32, equation (8.4.23.1)] and [30, equations (1.59-1.60)] on [33, equation (1)]. Fox's H-function is derived for α-μ/G distributions by following [30, equation (1.60)] and [34, equation (7)], for DSS from [36, equation (7)], for SSS from [36, equation (10)], for cascaded G-K from [35, equation (18)], while for N*Rayleigh from [38], for N*Nakagami-m from [39], for N*GK from [40], and for N*Fisher distributions from [41], which are derived with the aid of [32, equation (8.3.2.21)] and then [30, Property 1.3 & 1.5]. Finally, Fox's H for Gamma-Gamma distribution [37] is deduced with the aid of [32, equation (8.3.2.21)] and [30, Property 1.4, 1.3, & 1.5].

III. ASYMPTOTIC ANALYSIS

Asymptotic analysis has gained special attention during the past few years in system optimization [11]. In the literature, different methodologies are proposed for analysing the system performance attained at both low and high power, as detailed below:

In [11], Zhang et al. proposed a new asymptotic analysis framework, in which the PDF is first approximated around the origin and then different performance metrics are evaluated. This approach is well suited for most distributions, but it faces difficulties in diversity analysis associated with distributions having summation terms, as exemplified by the Mixture-Gamma [42], Weibull/Log-normal [43], and Mixture-Inverse Gaussian [44], [45] distributions. Peppas et al. [46] proposed asymptotic solutions for cognitive radio scenarios by approximating the results at high power, but their solutions exhibited limitations both when the PDF has a complex mathematical structure, and for spatial diversity techniques.

Additionally, asymptotic frameworks are capable of reducing the analytical complexity of diversity reception. The conventional approaches rely on the PDF at the origin, followed by averaging and using the AWGN and ALN contamination to derive the asymptotic expressions of the OP, average SEP, and average probability of detection. As a benefit, Fox's H-fading model will resolve the issues stated above. When $Z \to 0$ the expression given by (1), will have the structure given as [47, Corollary 3]

$$\mathcal{R}H_{\hat{p},\hat{q}}^{\hat{m},\hat{n}}\left[\mathcal{T}Z\right]_{Z\to 0} = \mathcal{R}h_j(\mathcal{T}Z)^{\Omega}, \tag{3}$$

where $\Omega = \min_{1\le j\le \hat{m}}\left[\frac{Re(f_j)}{F_j}\right]$ and h_j is evaluated using [47, Corollary 2] and is defined as

$$h_j = \frac{\prod_{i=1,i\neq j}^{\hat{m}}\Gamma\left(f_i - \frac{f_jF_i}{F_j}\right)\prod_{i=1}^{\hat{n}}\Gamma\left(1-e_i+\frac{f_jE_i}{F_j}\right)}{F_j\prod_{i=\hat{n}+1}^{\hat{p}}\Gamma\left(e_i-\frac{f_jE_i}{F_j}\right)\prod_{i=\hat{m}+1}^{\hat{q}}\Gamma\left(1-f_i-\frac{f_jF_i}{F_j}\right)}, \tag{4}$$

where h_j is listed in Table 5 for various Fox's H-fading channels. In the cases, where $\hat{m}>1$, h_j has numerous values, which hence requires the selection of the most appropriate parameters. The CDF of the expression given by (3) is evaluated by employing the identity $F_Y(\gamma) = \int_0^{\gamma} f_Y(\gamma)d\gamma$ and it is given by

$$F_Y(\gamma) = \frac{\mathcal{R}h_j\mathcal{T}^{\Omega}}{\Omega+1}\gamma^{\Omega+1}. \tag{5}$$

A. DIVERSITY ANALYSIS OF FOX'S H-DISTRIBUTION

In a communication system, the spurious effect of fading is often compensated by the inclusion of multiple antennas at the Tx or at the Rx or both, so that the QoS can be maintained. Various signal combining techniques are utilised in the open literature to improve the QoS. Among them, MRC, EGC, and SC are the most popular diversity schemes. The most complex MRC yields the best improvements, followed by EGC and SC. In this subsection, we highlight the PDF expressions of the above diversity schemes.

1) MRC DIVERSITY PDF

The MRC scheme combines the signal received from independent paths, which are first co-phased, then weighted by a corresponding weighting factor inversely proportional to their SNR, and finally added improve the instantaneous SNR of the combiner output. The MRC output may then be expressed as [48]

$$\gamma_{MRC} = \sum_{r=1}^{L}\gamma_r. \tag{6}$$

Taking the LT of (6), yields

$$M_{\gamma_{MRC}}(s) = \prod_{r=1}^{L}M_{\gamma_r}(s). \tag{7}$$

The MGF for the individual branch SNR is calculated by taking the LT of (3) with the aid of [49, 3.381.4], as given by

$$M_{\gamma}(s) = \mathcal{R}h_j\mathcal{T}^{\Omega}\frac{\Gamma(\Omega+1)}{s^{\Omega+1}}. \tag{8}$$

Substituting (8) into (7) and after some further algebraic manipulations, we arrive at:

$$M_{\gamma_{MRC}}(s) = \left\{\prod_{r=1}^{L}\mathcal{R}_rh_j\mathcal{T}^{\Omega_r}\Gamma(\Omega_r+1)\right\}\frac{1}{s^{\left(\sum_{r=1}^{L}\Omega_r\right)+L}}. \tag{9}$$

Upon multiplying the numerator and denominator of (9) by $\Gamma\left(\left(\sum_{r=1}^{L}\Omega_r\right)+L\right)$ and then taking the inverse LT, we get the desired origin PDF expression of

$$f_{\gamma_{MRC}}^{inid}(\gamma) = \mathcal{K}^{MRC}\gamma^{\Psi^{MRC}-1}, \tag{10}$$

where the parameters $\mathcal{K}^{MRC}$ and Ψ^{MRC} are defined in Table 6. Upon assuming L i.i.d. branches, and $\bar{\gamma}_1 = \bar{\gamma}_2 = \ldots\ldots = \bar{\gamma}_L = \bar{\gamma}$,

TABLE 5. h_j values for various Fox's H-fading channels.

Channel	$\hat{m}$	h_j
Maxwell	1	h_1=1
$\alpha-\mu$	1	$h_1=\frac{\alpha}{2}$
E G-G	2	$h_1=\xi\Gamma\left(\frac{\hat{r}_s\xi_s-\hat{r}\xi}{\xi_s}\right)$, $h_2=\xi_s\Gamma\left(\frac{\hat{r}\xi-\hat{r}_s\xi_s}{\xi}\right)$
F-S $\mathcal{F}$	1	$h_1=\Gamma(\hat{n}+\hat{m})$
GBK	2	$h_1=\hat{\lambda}\Gamma(n_G-m_G)$, $h_2=\hat{\lambda}\Gamma(m_G-n_G)$
α-μ/G	2	$h_1=\Gamma\left(\hat{k}-\mu+\frac{1}{\alpha}-1\right)$), $h_2=\Gamma\left(\mu-\hat{k}-\frac{1}{\alpha}+1\right)$)
SSS	2	$h_1=\Gamma(m_2-m_1)\Gamma(a_1+m_1)$, $h_2=\Gamma(m_1-m_2)\Gamma(a_1+m_2)$
DSS	2	$h_1=\Gamma(m_2-m_1)\Gamma(a_2+m_1)\Gamma(a_1+m_1)$, $h_2=\Gamma(m_1-m_2)\Gamma(a_2+m_2)\Gamma(a_1+m_2)$
Cascaded G-K	4	$h_1=\Gamma(\tilde{m}_1-\tilde{m}_{s1})\Gamma(\tilde{m}_{s2}-\tilde{m}_{s1})\Gamma(\tilde{m}_2-\tilde{m}_{s1})$, $h_2=\Gamma(\tilde{m}_{s1}-\tilde{m}_1)\Gamma(\tilde{m}_{s2}-\tilde{m}_1)\Gamma(\tilde{m}_2-\tilde{m}_1)$, $h_3=\Gamma(\tilde{m}_{s1}-\tilde{m}_{s2})\Gamma(\tilde{m}_1-\tilde{m}_{s2})\Gamma(\tilde{m}_2-\tilde{m}_{s2})$, $h_4=\Gamma(\tilde{m}_{s1}-\tilde{m}_2)\Gamma(\tilde{m}_1-\tilde{m}_2)\Gamma(\tilde{m}_{s2}-\tilde{m}_2)$
Gamma-Gamma	3	$h_1=\Gamma(\varsigma-\tilde{\xi}^2)\Gamma(\varpi-\tilde{\xi}^2)$, $h_2=\frac{\Gamma(\tilde{\xi}^2-\varsigma)\Gamma(\varpi-\varsigma)}{\Gamma(\tilde{\xi}^2+1-\varsigma)}$, $h_3=\frac{\Gamma(\tilde{\xi}^2-\varpi)\Gamma(\varsigma-\varpi)}{\Gamma(\tilde{\xi}^2+1-\varpi)}$
N-Rayleigh	N	h_i=1; $1\leq j\leq N$
N-Nakagami-m	N	$h_i=\prod_{i=1,i\neq j}^{N}\Gamma(m_i-m_j)$; $1\leq j\leq N$
N-GK	2N	$h_1=\Gamma(m_1-\tilde{m}_{s1})\Gamma(m_2-\tilde{m}_{s1})\Gamma(\tilde{m}_{s2}-\tilde{m}_{s1})....\Gamma(\tilde{m}_{sN}-\tilde{m}_{s1})\Gamma(m_N-\tilde{m}_{s1})$; $h_2=\Gamma(\tilde{m}_{s1}-m_1)\Gamma(m_2-m_1)\Gamma(\tilde{m}_{s2}-m_1)....\Gamma(\tilde{m}_{sN}-m_1)\Gamma(m_N-m_1)$; $h_3=\Gamma(\tilde{m}_{s1}-\tilde{m}_{s2})\Gamma(m_1-\tilde{m}_{s2})\Gamma(m_2-\tilde{m}_{s2})....\Gamma(\tilde{m}_{sN}-\tilde{m}_{s2})\Gamma(m_N-\tilde{m}_{s2})$; $h_{2N-1}=\Gamma(\tilde{m}_{s1}-\tilde{m}_{sN})\Gamma(m_1-\tilde{m}_{sN})\Gamma(\tilde{m}_{s2}-\tilde{m}_{sN})....\Gamma(m_{N-1}-\tilde{m}_{sN})\Gamma(m_N-\tilde{m}_{sN})$; $h_{2N}=\Gamma(\tilde{m}_{s1}-m_N)\Gamma(m_1-m_N)\Gamma(\tilde{m}_{s2}-m_N)....\Gamma(m_{N-1}-m_N)\Gamma(\tilde{m}_{sN}-m_N)$
N-Fisher	N	$h_j=\prod_{i=1,i\neq j}^{N}\Gamma(\hat{n}_i-\hat{n}_j)\prod_{i=1}^{N}\Gamma(\hat{n}_j-\hat{m}_i)$; $1\leq j\leq N$
N-α-$\mathcal{F}$	N	$h_j=\prod_{i=1,i\neq j}^{N}\Gamma(\Upsilon_i-\Upsilon_j)\prod_{i=1}^{N}\Gamma(\Upsilon_j-\Phi_i)$; $1\leq j\leq N$

(7) may be reformulated as

$$M_{\gamma_{MRC}}^{iid}(s)=\left[M_{\gamma_r}(s)\right]^L. \tag{11}$$

Upon substituting (8) into (11) and then employing the inverse LT, one obtains the origin PDF under the i.i.d. case associated with the same structure as given in (10). The respective parameters are illustrated in Table 6. In Fig. 1 the Fisher-Snedecor F origin power PDF is compared to the exact power PDF for different fading parameters. It is observed that the plots follow the exact PDF for a wide range of instantaneous SNRs. The multipath parameter n determines the slope of the power PDF at $\gamma\to 0$. However, as the shadowing parameter m_s and the average SNR are changed, there is a parallel shift in the figure.

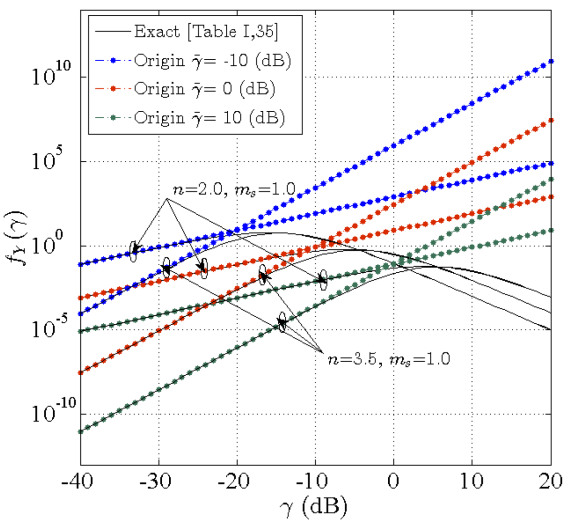

FIGURE 1. Fisher-Snedecor F distribution's origin and exact PDF.

2) EGC DIVERSITY PDF

Similar to MRC, the signals gleaned from L paths are co-phased, weighted with a factor of unity and then are summed

TABLE 6. Distribution parameters for MRC, EGC, and SC diversity schemes.

Distribution Parameters	i.n.i.d.	i.i.d.
$\mathcal{K}^{MRC}$	$\frac{\prod_{r=1}^{L}\left(\mathcal{R}_r h_j \mathcal{T}_r^{\Omega_r}\Gamma(\Omega_r+1)\right)}{\Gamma\left(\left(\sum_{r=1}^{L}\Omega_r\right)+L\right)}$	$\frac{\mathcal{R}^L h_j^L \mathcal{T}^{L\Omega}\left(\Gamma(\Omega+1)\right)^L}{\Gamma(\Omega L+L)}$
Ψ^{MRC}	$\left(\sum_{r=1}^{L}\Omega_r\right)+L$	$L(\Omega+1)$
$\mathcal{K}^{EGC}$	$\frac{\left\{\prod_{r=1}^{L}\left(2h_j\mathcal{R}_r\mathcal{T}_r^{\Omega_r}\Gamma(2\Omega_r+2)\right)\right\}L^{\sum_{r=1}^{L}(\Omega_r+1)}}{2\Gamma\left(\sum_{r=1}^{L}(2\Omega_r+2)\right)}$	$\frac{\left(2h_j\mathcal{R}\mathcal{T}^{\Omega}\Gamma(2\Omega+2)\right)^L L^{L(\Omega+1)}}{2\Gamma((2\Omega+2)L)}$
Ψ^{EGC}	$\sum_{r=1}^{L}(\Omega_r+1)$	$L(\Omega+1)$
$\mathcal{K}^{SC}$	$\left\{\sum_{r=1}^{L}(\Omega_r+1)\right\}\left\{\prod_{r=1}^{L}\left(\frac{\mathcal{R}_r h_j \mathcal{T}_r^{\Omega_r}}{\Omega_r+1}\right)\right\}$	$L\frac{\left(\mathcal{R}h_j\mathcal{T}^{\Omega}\right)^L}{(\Omega+1)^{L-1}}$
Ψ^{SC}	$\sum_{r=1}^{L}(\Omega_r+1)$	$L(\Omega+1)$

to get the combiner's output SNR as given below

$$\gamma_{EGC}=\left(\frac{1}{\sqrt{L}}\sum_{r=1}^{L}\sqrt{\gamma_r}\right)^2. \tag{12}$$

Taking the square root of both sides, yields

$$X_{EGC}=\sum_{r=1}^{L}\frac{X_r}{\sqrt{L}}. \tag{13}$$

Similarly to MRC, the MGF is expressed as

$$M_{X_{EGC}}(s)=\prod_{r=1}^{L}M_{X_r}\left(\frac{s}{\sqrt{L}}\right). \tag{14}$$

The envelope PDF for (3) is deduced by using the relationship of $P_Y(\gamma)=\frac{P_R\left(\sqrt{\frac{\hat{r}^2\gamma}{\bar{\gamma}}}\right)}{2\sqrt{\frac{\gamma\bar{\gamma}}{\hat{r}^2}}}$ [50, 2.3], yielding

$$f_X(x)=\frac{2\mathcal{R}h_j\mathcal{T}^{\Omega}\bar{\gamma}^{\Omega+1}}{\hat{x}^{2\Omega+2}}x^{2\Omega+1}. \tag{15}$$

Taking the LT of (15) results in

$$M_X\left(\frac{s}{\sqrt{L}}\right)=\frac{2\mathcal{R}h_j\mathcal{T}^{\Omega}\bar{\gamma}^{\Omega+1}\Gamma(2\Omega+2)}{\hat{x}^{2\Omega+2}\left(\frac{s}{\sqrt{L}}\right)^{2\Omega+2}}. \tag{16}$$

Substituting (16) into (14) and carrying out some further algebraic manipulations yields

$$M_{X_{EGC}}(s)=\left\{\prod_{r=1}^{L}\left(\frac{2h_j\mathcal{R}_r\mathcal{T}^{\Omega_r}\bar{\gamma}_r^{\Omega+1}\Gamma(2\Omega_r+2)}{\hat{x}^{2\Omega_r+2}}\right)\right\}\times\frac{L^{\sum_{r=1}^{L}(\Omega_r+1)}\Gamma\left(\sum_{r=1}^{L}(2\Omega_r+2)\right)}{\Gamma\left(\sum_{r=1}^{L}(2\Omega_r+2)\right)s^{\sum_{r=1}^{L}(2\Omega_r+2)}}. \tag{17}$$

Taking the inverse LT of (16) yields the origin envelope PDF of EGC reception, where the independent paths are non-identical

$$f_{X_{EGC}}^{inid}(x)=\left\{\prod_{r=1}^{L}\left(\frac{2h_j\mathcal{R}_r\mathcal{T}^{\Omega_r}\bar{\gamma}_r^{\Omega+1}\Gamma(2\Omega_r+2)}{\hat{x}^{2\Omega_r+2}}\right)\right\}\times\frac{L^{\sum_{r=1}^{L}(\Omega_r+1)}x^{\sum_{r=1}^{L}(2\Omega_r+2)-1}}{\Gamma\left(\sum_{r=1}^{L}(2\Omega_r+2)\right)}. \tag{18}$$

Finally, upon substituting the relationship given by [50, 2.3] into (18), the origin power PDF of EGC diversity reception is deduced similar by (10), where the parameters are defined in Table 6. Similarly to MRC, for i.i.d. the origin power PDF of EGC diversity reception will have a similar structure to (10) and the associated parameters are given in Table 6.

3) SC DIVERSITY PDF

In SC spatial diversity reception, the path having the highest SNR will be selected, thus the CDF is given by

$$F_{\gamma_{SC}}(\gamma)=\prod_{r=1}^{L}F_{\gamma_r}(\gamma). \tag{19}$$

Substituting (5) into (19) gives

$$F_{\gamma_{SC}}^{inid}(\gamma)=\left\{\prod_{r=1}^{L}\left(\frac{\mathcal{R}_r h_j\mathcal{T}^{\Omega_r}}{\Omega_r+1}\right)\right\}\gamma^{\sum_{r=1}^{L}(\Omega_r+1)-1}. \tag{20}$$

To derive the PDF expression, the above relationship has to be differentiated with respect to the parameter γ. It yields the origin PDF of SC diversity similar to the origin MRC PDF given by (10). For i.i.d. scenarios, the PDF of SC diversity is given by

$$f_{Y_{SC}}^{iid}(\gamma) = L\left[F_Y(\gamma)\right]^{L-1} f_Y(\gamma). \tag{21}$$

Upon substituting (3) and (5) into (21), one can obtain the origin PDF expression for SC diversity similar to (10). In Table 6, the fading parameters are illustrated both for i.n.i.d. and i.i.d. cases.

IV. PERFORMANCE METRICS

Wireless communication systems have diverse performance metrics, such as the OP, the average SEP, the probability of missed detection, etc. Our research primarily focuses on high-power approximations of the performance metrics using the origin PDF. Therefore, we have evaluated the OP and average SEP performance metrics for both SIMO and SISO systems.

A. OUTAGE PROBABILITY

The OP describes the probability that the received SNR is below the minimum threshold (γ_{th}), which is formulated as [43]

$$P_{out}(\gamma_{th}) = P[\gamma < \gamma_{th}] = \int_0^{\gamma_{th}} f_Y(\gamma) d\gamma. \tag{22}$$

Upon substituting (10) into (22), after some manipulations, we get

$$P_{out}(\gamma_{th}) = \frac{\mathcal{K}^D \gamma_{th}^{\Psi^D}}{\Psi^D}, \tag{23}$$

where D represents the MRC, EGC, and SC diversity parameters.

B. AVERAGE SEP

Noise is one of the main sources of signal impediments in the communication system. The level of impact on the data transmission can be quantified by the average SEP. In this subsection, we will presented the analytical expressions of results for both the coherent and non-coherent detection based average SEP. The analytical representation of SEP under a fading environment is deduced by averaging i.e. integrating $P_e(\gamma)$ across the entire dynamic range of the fading PDF $f_Y(\gamma)$ [43, (12)]

$$P\bar{(e)} = \int_0^{\infty} P_e(\gamma) f_Y(\gamma) d\gamma, \tag{24}$$

where $P_e(\gamma)$ is the SEP of non-fading environments.

1) COHERENT AVERAGE SEP

Here, we will consider the scenario where phase recovery at the Rx is possible in the face of both AWGN and ALN.

TABLE 7. SEP parameters for additive Laplacian noise.

Modulation Scheme	a	b	c
BPSK	$\frac{1}{2}$	0	2
QPSK	$\frac{3}{4}$	1	2

a) AWGN average SEP: Under AWGN the SEP of a non-faded environment is given by [43, Eq. (13)]

$$P_e(\gamma) = \hat{\mathcal{A}} erfc(\sqrt{\hat{\mathcal{B}}\gamma}), \tag{25}$$

where the constant parameters $\hat{\mathcal{A}}$ and $\hat{\mathcal{B}}$ are associated with different coherent modulation schemes defined in [51, Table I]. Upon substituting (25) and (10) into (24) and setting $\sqrt{\hat{\mathcal{B}}\gamma} = r$, we get

$$P\bar{(e)} = \frac{2\hat{\mathcal{A}}\mathcal{K}^D}{\hat{\mathcal{B}}^{\Psi^D}} \int_0^{\infty} t^{2\Psi^D - 1} erfc(t) dt. \tag{26}$$

Evidently, by the inclusion of [52, Eq. (2.8.2.1)], (26) can be simplified to

$$P\bar{(e)} = \frac{\hat{\mathcal{A}}\mathcal{K}^D}{\hat{\mathcal{B}}^{\Psi^D}\Psi^D\sqrt{\pi}} \Gamma\left(\frac{2\Psi^D + 1}{2}\right). \tag{27}$$

b) ALN average SEP: Under ALN, the average SEP statistics discussed here are of BPSK, QPSK, and M-ary PSK. The transmitted signal is detected using the MED based detector, rather than a maximum likelihood detector. The MED detector is simple and its SEP expressions are of low complexity. The conditional SEP of BPSK and QPSK is formulated as

$$P_e(\gamma) = \left(a + b\sqrt{\gamma}\right) e^{-c\sqrt{\gamma}}, \tag{28}$$

where the constants a and b are defined in [20] and for the sake of completeness are reproduced here in Table 7.

Upon substituting (10) and (28) into (24), as well as setting $\sqrt{\gamma} = t$, with the aid of [49, Eq. (3.381.4)], we have

$$P\bar{(e)} = \frac{2a\mathcal{K}^D\Gamma\left(2\Psi^D\right)}{c^{2\Psi^D}} + \frac{2b\mathcal{K}^D\Gamma\left(2\Psi^D + 1\right)}{c^{2\Psi^D + 1}}. \tag{29}$$

The conditional SEP of M-ary PSK for $M \geq 8$ is given as [20, Eq. (7)]

$$P_e(\gamma) = \frac{8}{M} \sum_{r=0}^{\frac{M}{4}-1} \mathcal{G}(r, \gamma) + \frac{2\tan\left(\frac{\pi}{M}\right)^2}{M\left(1 - \tan\left(\frac{\pi}{M}\right)^2\right)} e^{-2\sqrt{\gamma}}, \tag{30}$$

where

$$G(r, \gamma) = \frac{1}{2\mathcal{W}_1}\left(\mathcal{W}_1^2 e^{-\mathcal{K}_1\sqrt{\gamma}} - \mathcal{W}_2^2 e^{-\mathcal{K}_2\sqrt{\gamma}}\right) - \frac{\sin\left(\frac{2\pi}{M}\right)}{8\left(\cos\left(\frac{2\pi}{M}\right) + \sin\left(\frac{4r\pi}{M}\right)\right)} e^{-\mathcal{K}_3\sqrt{\gamma}}, \tag{31}$$

with $\mathcal{W}_1 = \cos\left((2r+1)\frac{\pi}{M}\right)$, $\mathcal{W}_2 = \sin\left((2r+1)\frac{\pi}{M}\right)$, $\mathcal{K}_1 = \frac{-2\sin\left(\frac{\pi}{M}\right)}{e^{\cos\left((2r+1)\frac{\pi}{M}\right)}}$, $\mathcal{K}_2 = \frac{-2\sin\left(\frac{\pi}{M}\right)}{e^{\sin\left((2r+1)\frac{\pi}{M}\right)}}$, and $\mathcal{K}_3 = 2\sqrt{2}\cos$

$\left(\frac{2r\pi}{M} - \frac{\pi}{M}\right)$. Utilizing the methodology of BPSK and QPSK, the SEP of M-ary PSK is deduced as follows

$$\begin{aligned} P(\bar{e}) =& \frac{8\mathcal{K}}{M} \sum_{r=0}^{\frac{M}{4}-1} \frac{\cos\left((2r+1)\frac{\pi}{M}\right)^2 \Gamma(2\Psi)}{\cos\left((2r+1)\frac{2\pi}{M}\right) \mathcal{K}_1^{2\Psi}} \\ &- \frac{8\mathcal{K}}{M} \sum_{r=0}^{\frac{M}{4}-1} \frac{\sin\left((2r+1)\frac{\pi}{M}\right)^2 \Gamma(2\Psi)}{\cos\left((2r+1)\frac{2\pi}{M}\right) \mathcal{K}_2^{2\Psi}} \\ &- \frac{8\mathcal{K}}{M} \sum_{r=0}^{\frac{M}{4}-1} \frac{\sin\left(\frac{2\pi}{M}\right) \Gamma(2\Psi)}{4\left(\cos\left(\frac{2\pi}{M}\right) + \sin\left(\frac{4r\pi}{M}\right) \mathcal{K}_3^{2\Psi}\right)} \\ &+ \frac{\tan\left(\frac{\pi}{M}\right)^2 \Gamma(2\Psi)}{M\left(1 - \tan\left(\frac{\pi}{M}\right)^2\right) 2^{2\Psi-1}}. \end{aligned} \tag{32}$$

2) NON-COHERENT AVERAGE SEP

Coherent detection requires perfect phase and channel state information at the Rx, which is hard to acquire. Therefore, non-coherent detection emerges as a low-complexity design for wireless sensor and relay networks [53]. Additionally, it is particularly beneficial for high Doppler SAGIN scenarios [54]. Specifically, it is beneficial because it reduces the system complexity and cost by eliminating channel estimation. Hence, we have derived the analytical expression of binary frequency shift keying, differential phase shift keying, and M-ary phase shift keying. The conditional SEP expression of AWGN is given by [43, Eq. (18)]

$$P_e(\gamma) = \mathcal{A}_n e^{-\mathcal{B}_n \gamma}, \tag{33}$$

where the constants $\mathcal{A}_n$ and $\mathcal{B}_n$ are given in [43, Table 2]. Upon substituting (10) and (33) into (24), with the aid of [49, Eq. (3.381.4)], we arrive at

$$P(\bar{e}) \approx \frac{\mathcal{A}_n \mathcal{K}^D \Gamma\left(2\Psi^D\right)}{\mathcal{A}_n^{2\Psi^D}}. \tag{34}$$

C. DIVERSITY GAIN AND SNR GAIN

Both the diversity gain and the SNR gain are important performance metrics that provide insights concerning the family of the diversity combining systems at high SNRs. The diversity gain determines the slope of the SEP curve, while the SNR gain measures the shift of the SEP curve relative to a benchmark SEP curve without changing its slope [11], [55], [56]. The SNR and diversity gains affect the OP and the average SEP as follows:

$$\begin{aligned} P_{out}(\gamma_{th}) &\approx \left(\mathcal{G}^{C_{op}} \bar{\gamma}\right)^{\mathcal{G}^{D_{op}}} \\ \bar{P}(e) &\approx \left(\mathcal{G}^{C_{Pe}} \bar{\gamma}\right)^{\mathcal{G}^{D_{Pe}}}, \end{aligned} \tag{35}$$

where the SNR and diversity gain parameters for the OP and average SEP are given by $\mathcal{G}^{C_{op}}$ & $\mathcal{G}^{C_{Pe}}$ and $\mathcal{G}^{D_{op}}$ & $\mathcal{G}^{D_{Pe}}$, respectively.

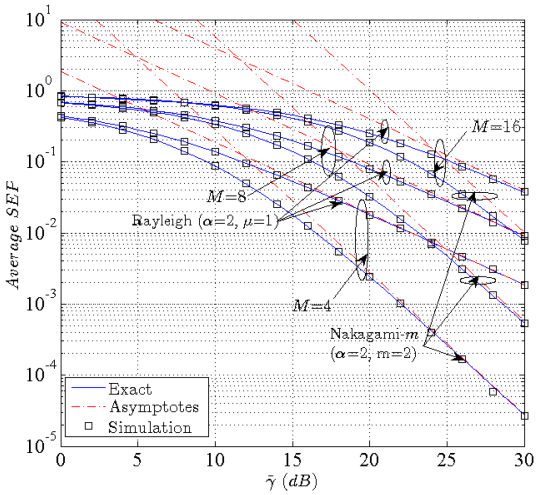

FIGURE 2. Average SEP of M-ary PAM for special cases of α-μ fading channel.

V. RESULTS AND DISCUSSIONS

The accuracy of the mathematical analysis presented in the previous sections requires validation. Hence, all the theoretical plots are compared to the Monte-Carlo simulation results with $\geq 10^6$ samples. Additionally, we also examine the impact of system parameters through different performance metrics, such as the OP and average SEP/BEP for a few special cases of Fox's H-functions, namely for the α-μ, Fisher-Snedecor F, GBK, and single shadowed scenarios.

In Fig. 2, the average SEP of coherent M-ary PAM has been plotted for the α-μ fading model. The figure contains exact (generated through integral simulation), asymptotic, and simulation results. To elaborate, Fig. 2 includes two special cases, namely the Rayleigh ($\alpha = 2$ & μ) and Nakagami-m ($\alpha = 2$ & $m = 2$ μ) scenarios, for $M = 4$, 8, and 16 conveying 2, 3, and 4 bits. The figure clearly demonstrates that as expected, an increase in the constellation size increases the SEP, the intra-constellation distance is reduced. It is further noted that the asymptotes coincide with the exact and simulation results.

Fig. 3 shows the average BEP for binary phase shift keying in the face of ALN for transmission over Fisher-Snedecor F distributed fading channels. The set of values considered for the Fisher-Snedecor F parameters n and m_s are in the range of $1 \rightarrow 15$. The figure includes plots for three special shadowing cases, such as intense shadowing ($n = 1$, $m_s = 1$), moderate shadowing ($n = 7$, $m_s = 7$), and light shadowing ($n = 15$, $m_s = 15$). As expected, shadowing has an adverse effect on the system. The SEP of 10^{-5} is achieved at about 16 (dB) for light shadowing, nearly 18 (dB) for moderate shadowing, and at a very high SNR beyond 30 (dB) for intense shadowing.

The average SEP plots for MRC and SC diversity are illustrated in Figs. 4 and 5. Explicitly, Fig. 4 plots the SEP of M-ary phase shift keying for transmission over GBK channels. Here, two i.i.d. branches are considered, and the parameters are as follows: $n = 2.5$, $m = 2$, $\lambda = 1.5$, for constellation sizes of $M = 8$ & 16. As expected, the increasing

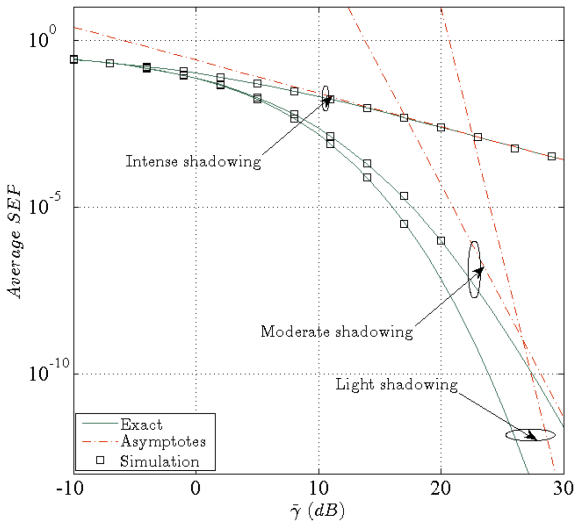

FIGURE 3. Average BEP of BPSK for Fisher-*F* fading under different shadowing with Additive Laplacian noise.

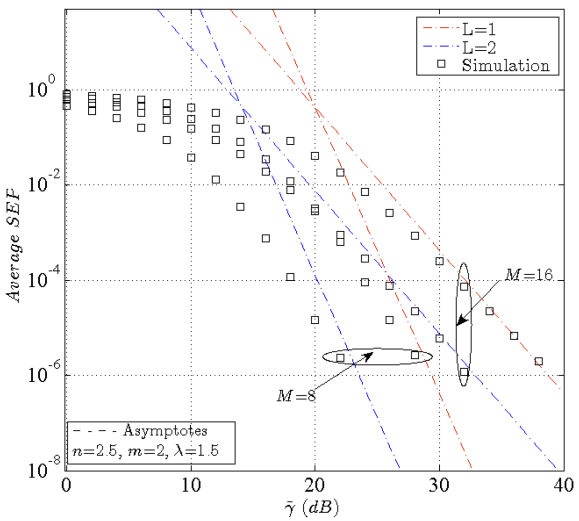

FIGURE 4. Average SEP of *M*-ary PSK for GBK distribution with MRC diversity.

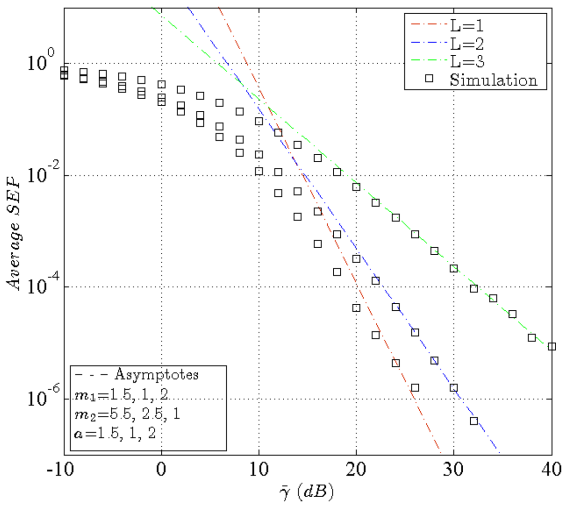

FIGURE 5. Average SEP of QPSK for SSS distribution with i.n.i.d. distributed branches.

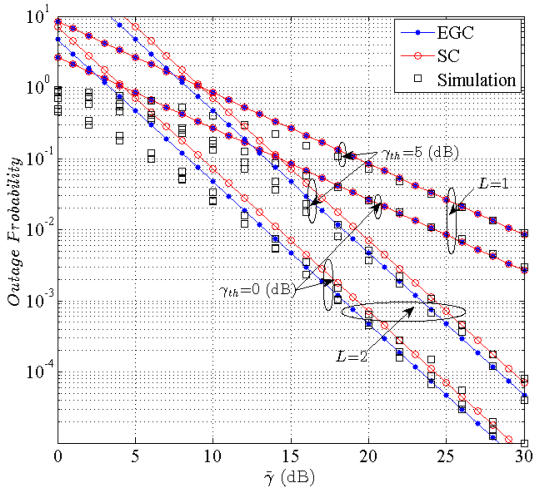

FIGURE 6. Outage probability for *N* cascaded Nakagami-*m* fading.

number of diversity branches improves the system's reliability. For example, to achieve SEP of 10^{-4}, SNRs of 25 (dB) and 18 (dB) are required for diversity orders of $L = 1$ and $L = 2$ respectively at $M = 8$. Similarly, SNRs of 32 (dB) and 27 (dB) are required for diversity orders of $L = 1$ and $L = 2$ at $M = 16$. It is further noted in Fig. 4 that a comparatively higher shift in SNR ($\sim$7 (dB)) is achieved at $M = 8$, while $\sim$5 (dB) will be observed for $M = 16$.

In Fig. 5, the average SEP plot for QPSK modulation scheme versus average SNR is plotted for the transmission over SSS model using SC diversity. Under this case, the individual branches are considered to be i.n.i.d., where $m_1 = \{1.5, 1, 2\}$, $m_2 = \{5.5, 2.5, 1\}$, $a = \{1.5, 1, 2\}$, and $L = \{1, 2, 3\}$. We observe that the error probability decreases upon increasing the diversity order. This is because as the number diversity paths increases, the combiner selects the specific path having the highest SNR. For example, to arrive at a SEP of 10^{-4}, the system having a single branch requires an average SNR of 28 (dB), while a dual-branch system requires an SNR of $\sim$22 (dB), and a triple-branch system needs 20 (dB). This explains why the initial diversity order increment has a significant contribution to the performance enhancement attained.

Fig. 6 shows the plots of OP for cascaded Nakagami-m fading channels with the aid of EGC and SC diversity schemes. The parameters considered here are as follows: $m_1 = 1.5$, $m_2 = 1$, threshold SNR, i.e., $\gamma_{th} = 0$ (dB) & 5 (dB), and the number of diversity paths is $L = 2$ & 3. The OP is typically reduced as the number of antennas at the Rx increases. This is due to the fact that systems with multiple antennas have higher SNR. It is further observed that the OP of EGC diversity is lower than that of SC diversity and it increases as the threshold SNR increases. For example, at an average SNR of 30 (dB), the probability of outage is 9×10^{-3} with $\gamma_{th} = 5$ (dB) and

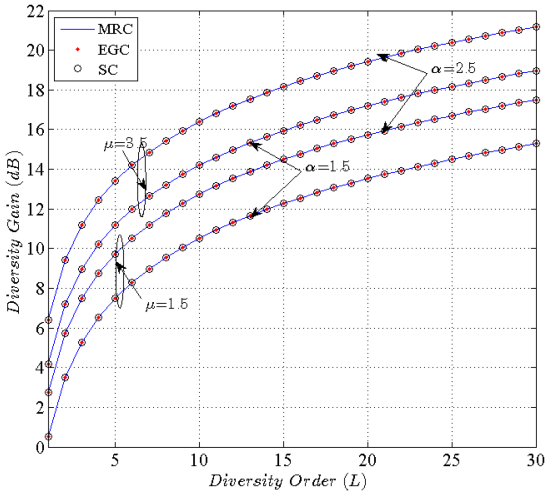

FIGURE 7. Diversity gain of OP versus L for α-μ fading with varying fading parameters.

2.9×10^{-3} with $\gamma_{th} = 0$ (dB), respectively. In all the plots, it has been verified that the asymptotes are in good agreement with the simulations at high SNRs, but depends on the choice of the fading parameters.

Fig. 7 depicts the plot of diversity gain against diversity order. The analytical expression for the diversity gain is given by $\mathcal{G}^{D_{op}} = L(\Omega + 1)$. It is observed from the plot and the expressions that all the diversity combining schemes have the same representation of diversity gain and are also independent of the OP threshold. It is further observed that the diversity gain increases as the fading parameters α and μ increase.

VI. SUMMARY AND CONCLUSION

Unified average SEP and OP results have been presented for generalised Fox's H-fading with spatial diversity. The entire body of work presented is based on the origin PDF, which produces performance results at a reduced complexity. The work also addressed the parameters of the origin PDF for some special cases of Fox's H-fading that are well suited for different wireless applications, namely, inter-vehicle communication, unmanned aerial communication, millimetre wave communication, etc. All the formulations derived are compared to numerical simulation results to quantify their precision.

REFERENCES

[1] Y. Abo Rahama, M. H. Ismail, and M. S. Hassan, "On the sum of independent fox's H-function variates with applications," *IEEE Trans. Veh. Technol.*, vol. 67, no. 8, pp. 6752–6760, Aug. 2018, doi: 10.1109/TVT.2018.2827180.

[2] M. M. H. El Ayadi and M. H. Ismail, "Unified approach for probability of detection evaluation over generalised fading channels," *IET Commun.*, vol. 10, no. 12, pp. 1532–1541, 2016.

[3] Y. Jeong, J. W. Chong, H. Shin, and M. Z. Win, "Intervehicle communication: Cox-fox modeling," *IEEE J. Sel. Areas Commun.*, vol. 31, no. 9, pp. 418–433, Sep. 2013, doi: 10.1109/JSAC.2013.SUP.0513038.

[4] Y. Aborahama, M. H. Ismail, and M. S. Hassan, "Novel methods for generating fox's H-function distributed random variables with applications," *IEEE Trans. Veh. Technol.*, vol. 68, no. 7, pp. 7150–7154, Jul. 2019, doi: 10.1109/TVT.2019.2916385.

[5] S. K. Yoo, S. L. Cotton, P. C. Sofotasios, M. Matthaiou, M. Valkama, and G. K. Karagiannidis, "The Fisher-Snedecor F distribution: A simple and accurate composite fading model," *IEEE Commun. Lett.*, vol. 21, no. 7, pp. 1661–1664, Jul. 2017.

[6] F. Yilmaz and M. S. Alouini, "A novel unified expression for the capacity and bit error probability of wireless communication systems over generalized fading channels," *IEEE Trans. Commun.*, vol. 60, no. 7, pp. 1862–1876, Jul. 2012, doi: 10.1109/TCOMM.2012.062512.110846.

[7] Y. Abo Rahama, M. H. Ismail, and M. S. Hassan, "Capacity of fox's H-function fading channel with adaptive transmission," *Electron. Lett.*, vol. 52, no. 11, pp. 976–978, May 2016, doi: 10.1049/el.2016.0511">.

[8] Z. Ji, C. Dong, Y. Wang, and J. Lu, "On the analysis of effective capacity over generalized fading channels," in *Proc. IEEE Int. Conf. Commun.*, 2014, pp. 1977–1983, doi: 10.1109/ICC.2014.6883613.

[9] L. Kong, G. Kaddoum, and H. Chergui, "On physical layer security over fox's H-function wiretap fading channels," *IEEE Trans. Veh. Technol.*, vol. 68, no. 7, pp. 6608–6621, Jul. 2019, doi: 10.1109/TVT.2019.2915017.

[10] P. S. Chauhan, S. Kumar, V. K. Upaddhyay, R. Mishra, B. Kumar, and S. K. Soni, "Performance analysis of ED over air-to-ground and ground-to-ground fading channels: A unified and exact solution," *Int. J. Electron. Commun.*, vol. 138, 2021, Art. no. 153839, doi: 10.1016/j.aeue.2021.153839.

[11] Z. Wang and G. B. Giannakis, "A simple and general parameterization quantifying performance in fading channels," *IEEE Trans. Commun.*, vol. 51, no. 8, pp. 1389–1398, Aug. 2003, doi: 10.1109/TCOMM.2003.815053.

[12] F. R. A. Parente and J. C. S. S. Filho, "Asymptotically exact framework to approximate sums of positive correlated random variables and application to diversity-combining receivers," *IEEE Wireless Commun. Lett.*, vol. 8, no. 4, pp. 1012–1015, Aug. 2019, doi: 10.1109/LWC.2019.2904032.

[13] B. Zhu, J. Cheng, J. Yan, J.-y. Wang, L. Wu, and Y. Wang, "A new asymptotic analysis technique for diversity receptions over correlated lognormal fading channels," *IEEE Trans. Commun.*, vol. 66, no. 2, pp. 845–861, Feb. 2018, doi: 10.1109/TCOMM.2017.2767039.

[14] A. S. Gvozdarev, " Closed-form and asymptotic BER analysis of the fluctuating double-Rayleigh with line-of-sight fading channel," *IEEE Wireless Commun. Lett.*, vol. 11, no. 7, pp. 1548–1552, Jul. 2022, doi: 10.1109/LWC.2022.3179900.

[15] A. Wojnar, "Unknown bounds on performance in Nakagami channels," *IEEE Trans. Commun.*, vol. 34, no. 1, pp. 22–24, Jan. 1986.

[16] H. Hashemi, J. Haghighat, M. Eslami, and W. A. Hamouda, "Analysis of equal gain combining over fluctuating two-ray channels with applications to millimeter-wave communications," *IEEE Trans. Veh. Technol.*, vol. 69, no. 2, pp. 1751–1765, Feb. 2020, doi: 10.1109/TVT.2019.2959877.

[17] H. Li, Y. Wang, F. Guo, J. Wang, B. Wang, and C. Wu, "Differential privacy location protection method based on the Markov model," *Wireless Commun. Mobile Comput.*, vol. 2021, pp. 1–12, 2021, doi: 10.1155/2021/4696455.

[18] H. Soury and M.-S. Alouini, "On the symbol error rate of M-ary MPSK over generalized fading channels with additive Laplacian noise," in *Proc. IEEE Int. Symp. Inf. Theory*, 2014, pp. 2879–2883, doi: 10.1109/ISIT.2014.6875360.

[19] H. Soury and M. S. Alouini, "Symbol error rate of MPSK over EGK channels perturbed by a dominant additive Laplacian noise," *IEEE Trans. Commun.*, vol. 63, no. 7, pp. 2511–2523, Jul. 2015, doi: 10.1109/TCOMM.2015.2438813.

[20] O. S. Badarneh, "Error rate analysis of M-ary phase shift keying in α-η-μ fading channels subject to additive Laplacian noise," *IEEE Commun. Lett.*, vol. 19, no. 7, pp. 1253–1256, Jul. 2015, doi: 10.1109/LCOMM.2015.2423277.

[21] T. B. Santoso and M. Huda, "Performance analysis of BPSK system in the underwater acoustic channel with additive Laplacian noise," in *Proc. IEEE Int. Electron. Symp. Eng. Technol. Appl.*, 2017, pp. 75–80, doi: 10.1109/ELECSYM.2017.8240382.

[22] L. Kong, G. Kaddoum, and Z. Rezki, "Highly accurate and asymptotic analysis on the SOP over SIMO α-μ fading channels," *IEEE Commun. Lett.*, vol. 22, no. 10, pp. 2088–2091, Oct. 2018, doi: 10.1109/LCOMM.2018.2861877.

[23] P. S. Chauhan, S. Kumar, V. K. Upaddhyay, and S. K. Soni, "Unified approach to effective capacity for generalised fading channels," *Phys. Commun.*, vol. 45, Apr. 2021, Art. no. 101278.

[24] X. Wang, W. Cheng, and X. Xu, "On the exact and asymptotic analysis of wireless transmission over α-μ/Inverse gamma composite fading channels," in *Proc. IEEE Int. Conf. Wireless Commun. Signal Process.*, 2020, pp. 789–794.

[25] R. Maurya, P. S. Chauhan, S. Srivastava, S. K. Soni, and B. Mishra, "Energy detection investigation over composite α-μ/inverse-gamma wireless channel," *Int. J. Electron. Commun.*, vol. 130, Feb. 2021, Art. no. 153556.

[26] P. S. Chauhan, S. Kumar, and S. K. Soni, "Performance analysis of non-identical cascaded α-μ fading channels," *Wireless Pers. Commun.*, vol. 116, pp. 3553–3566, 2021.

[27] A. M. Magableh, T. Aldalgamouni, O. Badarneh, S. Mumtaz, and S. Muhaidat, "Performance of non-orthogonal multiple access (NOMA) systems over N-Nakagami-*m* multipath fading channels for 5G and beyond," *IEEE Trans. Veh. Technol.*, vol. 71, no. 11, pp. 11615–11623, Nov. 2022, doi: 10.1109/TVT.2022.3189589.

[28] A. A. Khuwaja, Y. Chen, N. Zhao, M. S. Alouini, and P. Dobbins, "A survey of channel modeling for UAV communications," *IEEE Commun. Surveys Tuts.*, vol. 20, no. 4, pp. 2804–2820, Fourthquarter 2018.

[29] F. Yilmaz and M. S. Alouini, "A new simple model for composite fading channels: Second order statistics and channel capacity," in *Proc. IEEE 7th Int. Symp. Wireless Commun. Syst.*, 2010, pp. 676–680.

[30] A. Mathai, R. K. Saxena, and H. J. Haubold, *The H-Function: Theory and Applications*, 1st ed., Berlin, Germany: Springer, 2010.

[31] O. S. Badarneh, "Statistics of the product of two α-$\mathcal{F}$ variates with applications," *IEEE Commun. Lett.*, vol. 25, no. 6, pp. 1761–1765, Jun. 2021, doi: 10.1109/LCOMM.2021.3062598.

[32] A. P. Prudnikov, Y. A. Brychkov, and O. I. Marichev, *Integrals and Series* (More Special Functions Series), vol. 3, 1st ed., Philadelphia, PA, USA: Gordon Breach Sci. Publishers, 1986.

[33] P. S. Chauhan et al., "Performance analysis of wireless communication system over non-identical cascaded generalised gamma fading channels," *Int. J. Commun. Syst.*, vol. 32, 2019, Art. no. e4004, doi: 10.1002/dac.4004.

[34] O. S. Badarneh, "Performance evaluation of wireless communication systems over composite α-μ/Gamma fading channels," *Wireless Pers. Commun.*, vol. 17, pp. 1235–1249, 2017.

[35] X. Chen, X. Hu, Q. Zhu, W. Zhong, and B. Chen, "Channel modeling and performance analysis for UAV relay systems," *China Commun.*, vol. 15, no. 12, pp. 89–97, Dec. 2018.

[36] P. S. Bithas, V. Nikolaidis, A. G. Kanatas, and G. K. Karagiannidis, "UAV-to-ground communications: Channel modeling and UAV selection," *IEEE Trans. Commun.*, vol. 68, no. 8, pp. 5135–5144, Aug. 2020.

[37] I. S. Ansari, F. Yilmaz, and M. Alouini, "Performance analysis of FSO links over unified gamma-gamma turbulence channels," in *Proc. IEEE 81st Veh. Technol. Conf.*, 2015, pp. 1–5.

[38] P. C. Sofotasios, L. Mohjazi, S. Muhaidat, M. Al-Qutayri, and G. K. Karagiannidis, "Energy detection of unknown signals over cascaded fading channels," *IEEE Antennas Wireless Propag. Lett.*, vol. 15, pp. 135–138, 2016.

[39] G. K. Karagiannidis, N. C. Sagias, and P. T. Mathiopoulos, "N∗Nakagami: A novel stochastic model for cascaded fading channels," *IEEE Trans. Commun.*, vol. 55, no. 8, pp. 1453–1458, Aug. 2007.

[40] I. Trigui, A. Laourine, S. Affes, and A. Stephenne, "On the performance of cascaded generalized K fading channels," in *Proc. IEEE Glob. Telecommun. Conf.*, 2009, pp. 1–5.

[41] O. S. Badarneh, S. Muhaidat, P. C. Sofotasios, S. L. Cotton, K. Rabie, and D. B. da Costa, "The N∗Fisher-Snedecor F cascaded fading model," in *Proc. IEEE 14th Int. Conf. Wireless Mobile Comput. Netw. Commun.*, 2018, pp. 1–7.

[42] P. S. Chauhan and S. K. Soni, "Performance analysis of dual branch MRC diversity over non-identical mixture of gamma distribution," in *Proc. IEEE 5th Uttar Pradesh Sect. Int. Conf. Elect., Electron. Comput. Eng.*, 2018, pp. 1–4.

[43] P. S. Chauhan, D. Tiwari, and S. K. Soni, "New analytical expressions for the performance metrics of wireless communication system over Weibull/Lognormal composite fading," *Int. J. Electron. Commun.* vol. 82, pp. 397–405, 2017.

[44] P. S. Chauhan, P. Negi, and S. K. Soni, "A unified approach to modelling of probability of detection over α-μ/IG, κ-μ/IG, and η-μ/IG composite fading channels with application to cooperative system," *Int. J. Electron. Commun.*, vol. 87, pp. 33–42, 2017.

[45] S. Kumar, P. S. Chauhan, P. Raghuvanshi, and M. Kaur, "ED performance over α-η-μ/IG and α-κ-μ/IG generalized fading channels with diversity reception and cooperative sensing: A unified approach," *Int. J. Electron. Commun.*, vol. 97, pp. 273–279, 2018, doi: 10.1016/j.aeue.2018.10.027.

[46] K. P. Peppas, G. Efthymoglou, V. A. Aalo, M. Alwakeel, and S. Alwakeel, "Energy detection of unknown signals in Gamma-shadowed Rician fading environments with diversity reception," *IET Commun.*, vol. 9, no. 2, pp. 196–210, Jan. 2015.

[47] A. A. Kilbas and M. Saigo, "On the H-function," *Int. J. Stochastic Anal.*, vol. 12, pp. 1–14, 1999, doi: 10.1155/S1048953399000192.

[48] P. S. Chauhan, S. Kumar, and S. K. Soni, "New approximate expressions of average symbol error probability, probability of detection and AUC with MRC over generic and composite fading channels," *Int. J. Electron. Commun.*, vol. 99, pp. 119–129, 2019.

[49] I. S. Gradshteyn and I. M. Ryzhik, *Table of Integrals, Series, and Products*, 6th ed., New York, NY, USA: Academic, 2000.

[50] M. K. Simon and M. S. Alouini, *Digital Communication Over Fading Channels: A Unified Approach to Performance Analysis*. Hoboken, NJ, USA: Wiley, 2000.

[51] O. S. Badarneh and M. S. Aloqlah, "Performance analysis of digital communication systems over α-η-μ fading channels," *IEEE Trans. Veh. Technol.*, vol. 65, no. 10, 7972–7981, Oct. 2016, doi: 10.13140/RG.2.1.4046.7925.

[52] A. P. Prudnikov, Y. A. Brychkov, and O. I. Marichev, *Integrals and Series* Volume 2: Special Functions 1st ed., Philadelphia, PA, USA: Gordon Breach Sci. Publishers, 1986.

[53] B. Selim et al., "Performance analysis of coherent and non-coherent modulation under I/Q imbalance effects," *IEEE Access*, vol. 9, pp. 36125–36139, 2021, doi: 10.1109/ACCESS.2020.3028869.

[54] C. Xu et al., "Sixty years of coherent versus non-coherent tradeoffs and the road from 5G to wireless futures," *IEEE Access*, vol. 7, pp. 178246–178299, 2019, doi: 10.1109/ACCESS.2019.2957706.

[55] B. Zhu, J. Yan, Y. Wang, L. Wu, and J. Cheng, "Asymptotically tight performance bounds of diversity receptions over α-μ fading channels with arbitrary correlation," *IEEE Trans. Veh. Technol.*, vol. 66, no. 9, pp. 7619–7632, Sep. 2017, doi: 10.1109/TVT.2017.2686700.

[56] H. Ding, J. Ge, D. B. da Costa, and Z. Jiang, "Asymptotic analysis of cooperative diversity systems with relay selection in a spectrum-sharing scenario," *IEEE Trans. Veh. Technol.*, vol. 60, no. 2, pp. 457–472, Feb. 2011, doi: 10.1109/TVT.2010.2100053.

PUSPRAJ SINGH CHAUHAN was born in UP, India. He received the Bachelor of Technology degree in electronics and communication engineering from Uttar Pradesh Technical University, Lucknow, India, in 2009, the M. Tech. degree in digital signal processing from Govind Ballabh Pant Engineering College, Pauri, Uttarakhand, India, in 2011, and the Ph.D. degree in wireless communication in 2021. He is currently an Assistant Professor with the Pranveer Singh Institute of Technology, Kanpur, India. His research interests include wireless communication, propagation channel modeling, and Internet of Things. He was the recipient of the Best Paper Award with UPCON 2018, Gorakhpur. He is also a reviewers of various international journals, such as IEEE, Elsevier, Springer, and Wiley.

SANDEEP KUMAR (Senior Member, IEEE) received the B.Tech. degree in electronics and communication from Kurukshetra University, Thanesar, India, in 2004, and the Master of Engineering degree in electronics and communication from Thapar University, Patiala, India, in 2007, and the Ph.D. from Delhi Technological University, Delhi, India, in 2018. He is currently the Member (Senior Research Staff) with Central Research Laboratory, Bharat Electronics Limited, Ghaziabad, India. His research interests include the study of wireless channels, performance modeling of fading channels and cognitive radio networks. He was the recipient of various awards and certificates of appreciation for his research activities. He is also a Reviewer for IEEE, Elsevier, and Springer journals.

ANKIT JAIN received the Bachelor of Technology degree in electronics and instrumentation engineering from Uttar Pradesh Technical University, Lucknow, India, in 2007, and the M.Tech. degree in electronics instrumentation and control engineering (with Hons.) from National Institute of Technical Teachers Training and Research, Chandigarh, India. He is currently an Assistant Professor with the Department of Electronics and Communication, Pranveer Singh Institute of Technology, Kanpur, India. He has two patents granted in his credit. His main area of research is embedded systems and Internet of things (IoT), and wireless communication.

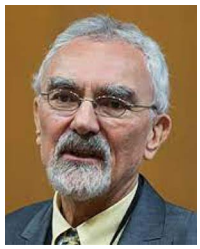

LAJOS HANZO (Life Fellow, IEEE) received Honorary Doctorates from the Technical University of Budapest, Budapest, Hungary, and Edinburgh University, Edinburgh, U.K., respectively. He is currently a Foreign Member of the Hungarian Science-Academy, Fellow of the Royal Academy of Engineering (FREng), IET, of EURASIP and holds the IEEE Eric Sumner Technical Field Award.